

Online Monitoring of Object Detection Performance During Deployment

Quazi Marufur Rahman, Niko Sünderhauf and Feras Dayoub

Abstract—During deployment, an object detector is expected to operate at a similar performance level reported on its testing dataset. However, when deployed onboard mobile robots that operate under varying and complex environmental conditions, the detector’s performance can fluctuate and occasionally degrade severely without warning. Undetected, this can lead the robot to take unsafe and risky actions based on low-quality and unreliable object detections. We address this problem and introduce a cascaded neural network that monitors the performance of the object detector by predicting the quality of its mean average precision (mAP) on a sliding window of the input frames. The proposed cascaded network exploits the internal features from the deep neural network of the object detector. We evaluate our proposed approach using different combinations of autonomous driving datasets and object detectors.

I. INTRODUCTION

Object detection plays a vital role in many robotics and autonomous system applications. For instance, a driverless car is expected to detect important objects such as vehicles, people and traffic signs accurately all the time. Failure to do so can cause severe consequences for the car and the people involved. Hence, there is ongoing research [1]–[10] to improve the robustness and accuracy of object detection systems. In general, an object detection system is trained and evaluated using non-overlapping training, validation, and test splits of a dataset before deployment. The underlying assumption is that the images encountered during deployment follow a similar distribution to the images presented before deployment. However, in the case of autonomous systems, the deployment environment can exhibit many conditions that are not well represented in the training and evaluation datasets. This leads to the fact that during the deployment phase, performance can fluctuate and may diverge from the expected training and evaluation phase performance without any prior warning. Such silent change in performance during the deployment phase is a serious concern for any vision-based robotic system, see Fig. 1.

The ultimate solution to meet this challenge is to develop a remarkably persistent object detection system by collecting training data from all imaginable conditions that can be encountered during the deployment phase. As such a solution is not practical, one remedy to this situation is to deploy a performance monitoring system for the object detector that

The authors are with the Australian Centre for Robotic Vision at Queensland University of Technology (QUT), Brisbane, QLD 4001, Australia. This research has been conducted by the Australian Research Council (ARC) Centre of Excellence for Robotic Vision (Grant CE140100016). The authors acknowledge continued support from the QUT Centre for Robotics. Contact: quazi.rahman@qut.edu.au

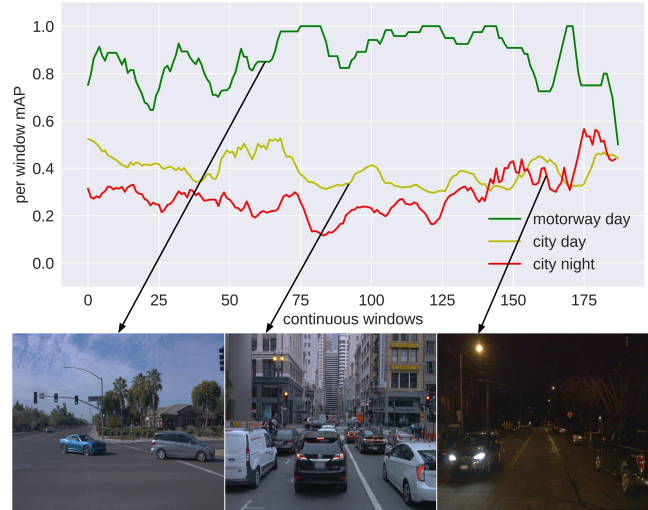


Fig. 1: Object detector performance deployed on a self-driving car depends heavily on multiple factors like traffic density, road type, and time of the day. The fluctuation in the mAP (calculated over a sliding window of 10 frames) shows the performance instability during the deployment phase in multiple places and conditions. We show that a specialized performance monitoring network can predict the mAP of the object detector to inform downstream tasks of its expected reliability. In this figure, the 1st row shows the continuous per-window mAP of three road scenes (motorway day, city day and night). The 2nd row shows one sample image from each road scene.

can raise warnings when the performance drops below a critical threshold.

A performance monitoring system is expected to provide the capability of self-assessment to the object detector. This self-assessment can improve safety and robustness during the deployment by monitoring the performance continuously and allowing to take preventive measures when the performance drops below the expected level.

To this end, the contribution of this paper is a novel cascaded neural network that exploits the internal feature maps from the deep neural network of the object detector for the task of online performance monitoring. Our proposed cascaded network operates on a sliding window of frames and continuously predicts the performance of the object detector in terms of mean average precision (mAP). We evaluate our proposed approach against multiple baselines using different combinations of datasets and object detection networks.

The rest of the paper is organized as follows: In Section II, we review the related works on performance monitoring. In Section III, we introduce our method for online performance monitoring of object detection during the deployment phase. Section IV outlines our experimental setup. Section V presents the results and finally in Section VI we draw conclusion for this work.

II. RELATED WORKS

Self-assessment and performance monitoring in robotics applications are important due to the high requirements of safety and robustness. In [11], a framework called robotic introspection is developed to provide a self-assessment mechanism for field robots during exploration and mapping of subterranean environments. Later [12] and [13] extended this work for obstacle avoidance and semantic mapping assessment. These works examine the output of the underlying models to predict their expected performance.

Another approach to address the performance monitoring problem is to evaluate model input before inference. [14] proposed a framework following this paradigm. They train an alert module to find cases where the target model will fail. Later, a similar approach was used for failure prediction for MAV [15], hardness predictor [16] for image classifiers, and probabilistic performance monitoring for robot perception system [17] for the task of pedestrian detection based on past experience from repeated visits to the same location.

Exploiting model confidence and uncertainty is another line of research to monitor the performance of a target model. Trust score [18], maximum class probability [19] and true class probability [20] are some recent works based on model confidence to identify the failure of an underlying image classifier. In the context of uncertainty estimation, [21] proposed to use dropout as a Bayesian approximation technique to represent model uncertainty. Later, [22], [23] applied this idea to identify the quality of image and video segmentation network. Out-of-distribution (OOD) detection [24]–[28] is another relevant field of research that can be useful for performance monitoring. While OOD detection focuses on identifying previously unknown input to a model, performance monitoring emphasizes identifying model accuracy for each-and-every input.

In the object detection context, there are few works that address the performance monitoring to some extent. [29] and [30] use dropout sampling and hard false positive mining, respectively, to identify object detection failures. [31] and [32] use internal and handcrafted features of an object detector respectively to identify false negative instances during deployment. These works focus on a per-object and per-frame basis and do not provide an overall assessment of the object detector performance considering the combined aspects of false positives, false negatives and object localization accuracy. These aspects are captured by a summary metric such as mAP. Our proposed approach can monitor object detection performance online by predicting the quality of its mAP for a sequence of images during the deployment phase without using any ground-truth data.

III. APPROACH OVERVIEW

In this section, we present our approach to online monitoring of object detection performance during the deployment phase. We start by formalizing the problem. Then we describe our proposed cascaded neural network architecture that operates on the feature stream generated by the underlying object detection network to monitor its performance in real-time.

Let us denote an object detection network as od_{net} , which is deployed on a driverless car to detect objects of interest like vehicle and pedestrian from the road. It takes a continuous stream of images $I = \{I_1, I_2, \dots, I_N\}$ and detects all possible objects from each I_i . Our goal is to monitor the performance of od_{net} by predicting its mAP continuously over a sliding window of images.

As described by [33], modern deep CNN’s become unstable when the input image is translated, re-scaled or slightly transformed by any other means. This observation holds for object detectors deployed on a driverless car too, where the mAP between two consecutive frames might vary significantly because of irrelevant and negligible changes in the viewpoint. As a result, per-frame performance monitoring can raise unnecessary false alarms. To mitigate this issue, we are adopting per sliding window performance monitoring, where the mAP between two consecutive windows does not change drastically. Hence, the performance monitoring network is expected to produce a consistent prediction by examining a sequence of images. To achieve this, we will deploy a second convolutional neural network that will access the internal features of od_{net} to predict the quality of the mAP for each sliding window of images. This second network will be referred to as the performance monitoring network, pm_{net} .

Instead of processing each input image I_i like od_{net} does at a time, pm_{net} operates on ω sequential images and predict the overall mAP of od_{net} on these ω images. We will use ω to refer to the window size used by pm_{net} . Here, pm_{net} takes a stream of windows $W = \{W_1, W_2, \dots, W_M\}$ and monitor the performance for each W_j , where $W_j = \{I_i, I_{i+1}, \dots, I_{i+\omega}\}$.

We formulate the task of performance monitoring as a multi-class classification problem consisting of C classes. To do so, the per-window mAP range is split into C equal and consecutive parts and labelled from 0 to $C - 1$. We will denote these per-window mAP labels using mAP_w . The lowest and the highest label, 0 and $C - 1$, refer to the worst and the best possible classes, respectively. As there is an ordinal relation among these labels, we will consider this multi-class classification problem as ordinal classification [34].

Our proposed pm_{net} exploits the features generated by od_{net} during per frame inference. od_{net} uses a backbone architecture B to extract features for the inference task where B is a collection of interconnected convolutional layers. During the inference, for each image I_i , B generates a set of p feature maps, $L_i = \{L_{i1}, L_{i2}, \dots, L_{ip}\}$. Here, shape of

L_{ij} is $c_{ij} \times h_{ij} \times w_{ij}$. c_{ij} , w_{ij} and h_{ij} are the channel, width and height of the j^{th} convolutional layer of the i^{th} image.

After each inference pm_{net} extracts L_i from B for input I_i and applies channel-wise average pooling to convert each 3D features into 2D. Now the converted set of feature is $\bar{L}_i = \{\bar{L}_{i1}, \bar{L}_{i2}, \dots, \bar{L}_{ip}\}$ and shape of \bar{L}_{ij} is $1 \times h_{ij} \times w_{ij}$. These operations are performed for all I_i and the newly formed corresponding 2D features are stacked together in channel-wise direction. That means the $\bar{L}_{(i+1)j}$ is stacked with \bar{L}_{ij} . After processing ω images we get the feature F_{W_i} for W_i . Here $F_{W_i} = \{F_1, F_2, \dots, F_p\}$ and F_i has the size of $\omega \times h_{ij} \times w_{ij}$. The task of pm_{net} is to predict mAP_w from F_W .

We design the pm_{net} as a cascaded convolutional neural network to train it to predict mAP_w from F_W . Here, each layer of pm_{net} is implicitly connected with all the previous layers through their individual convolutional filter. Using this network, we exploit the rich multi-level semantic features generated by the od_{net} instead of only using the last convolutional layer features. pm_{net} uses a set of convolutional filters $f = \{f_1, f_2, \dots, f_{p-1}\}$ to propagate the features of F_W from one layer to the next. Each filter f_i operates on F_i to generate a new feature \bar{F}_i which has the same shape of F_{i+1} . Now a concatenation is performed to join \bar{F}_i and F_{i+1} in channel-wise direction. This set of operations can be formulated using Equation 1.

$$\mathcal{F} = f_i(F_i) \oplus F_{i+1}; \quad i = 1, 2, \dots, p-1 \quad (1)$$

Next, we apply the adaptive average pooling operation on \mathcal{F} to generate a one dimensional feature vector. This feature is passed through subsequent fully connected layers to generate the final prediction for F_W . See Fig. 2 for a visualization of these procedures.

IV. EXPERIMENTAL SETUP

In this section, we will describe the settings that we used to evaluate our proposed approach.

A. Experimental Steps

We can describe the overall experimental procedure using three steps. At first, an object detector is trained using transfer learning techniques to detect different objects (vehicle, pedestrian) from a dataset named as *primary* training dataset. In the next step, the detector is used to detect similar objects from another dataset (*secondary* training dataset) which was not used during the initial training phase. This *secondary* training dataset consists of a stream of images. In this step, a sequential stream of images is fed to the object detector, and for each consecutive window of images, we collect the features for each window and calculate the corresponding mAP using the *secondary* training dataset as ground-truth. Then, we train the proposed cascaded CNN, pm_{net} to predict the mAP from the collected per-window features. Next, we use multiple metrics and another image stream dataset (*test* dataset unused in previous steps to evaluate the proposed approach. See Fig. 3 for a high-level overview of these steps.

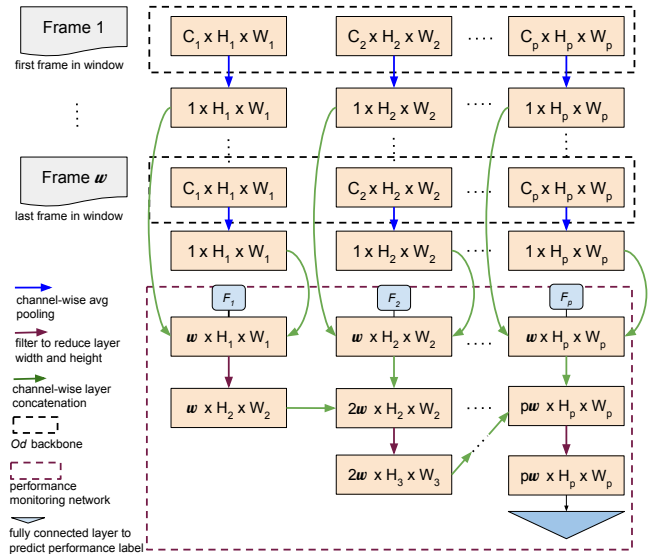


Fig. 2: Cascaded architecture of the proposed performance monitoring network. The first four rows show the procedure to convert the 3D feature from frame 1 to ω into 2D. These features are collected from the object detection backbone. 5th row demonstrates how the 2D features from corresponding layers are stacked together to generate a ω channel 3D feature. 6th and 7th rows represent how each feature is cascaded with the previous one.

B. Dataset

We used multiple combinations of three different datasets (KITTI [35], BDD [36], Waymo [37]) to conduct all the experiments. In each setting, one dataset from KITTI and BDD has been used as *primary* training dataset. Then we used one of the video datasets from KITTI, BDD and Waymo as the *secondary* training dataset, which was not a part of *primary* training dataset. To evaluate the system, we used one video dataset unused as *primary* or *secondary* training dataset. Each of the KITTI and BDD dataset has been split into 60%, 20% and 20% ratios to use as the *primary*, *secondary* and *test* dataset. Besides, 50 video segments of the Waymo dataset have been used as the *test* dataset. The idea of *primary* and *secondary* datasets have been introduced to demonstrate the distribution shift between the training and deployment phase in the case of a driverless car. Moreover, the performance monitoring network has been trained using the *secondary* dataset instead of *primary* dataset following the frameworks proposed by [14] and [15].

C. Training

We trained two-stage Faster RCNN [2] and one-stage RetinaNet [38] object detection networks pre-trained on MS-COCO [39] dataset to detect vehicle and pedestrian from the KITTI and BDD dataset. Both of these networks use ResNet50 [40] as their backbone. To be interoperable among multiple datasets, classes like car, van, tram and bus have been assigned to vehicle class. Besides, pedestrian and person classes from all the datasets are denoted as the

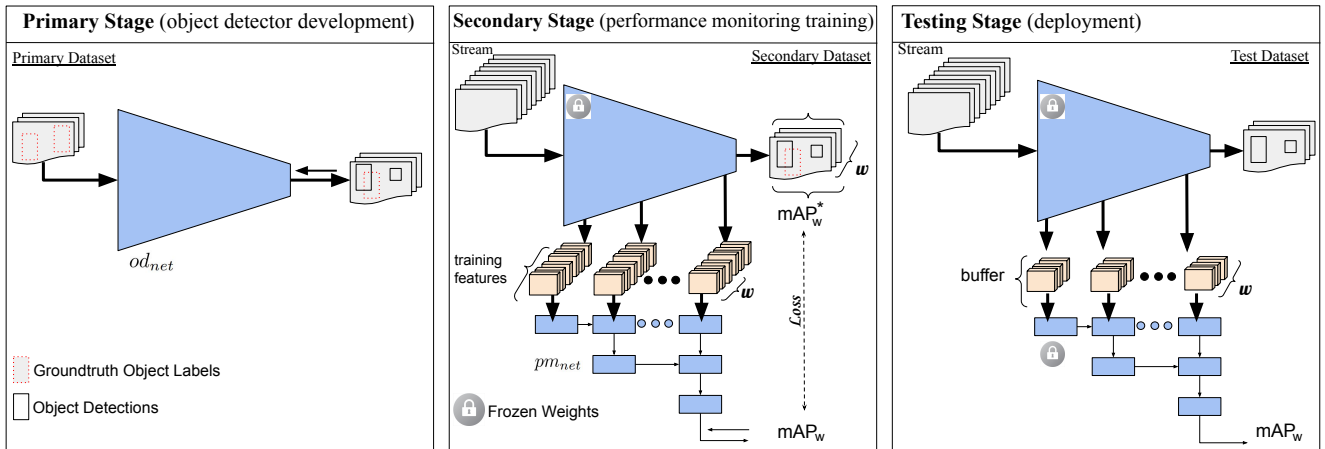


Fig. 3: An overview of the three stages for training and testing our performance monitoring network (pm_{net}). First, the object detector is developed using a *primary* training dataset. After the training is done, a *secondary* training dataset consisting of video streams is used to collect inner features from the backbone network of the object detector and train pm_{net} to predict the quality of the detector’s per-window mAP. Finally, a third *test* dataset of video streams is used to evaluate the performance monitoring network. The three datasets are independent of each other.

pedestrian class. Moreover, objects less than 25 pixels in width or height are removed from all the datasets.

To generalize the object detection and performance monitoring network across multiple kinds of weather, lighting conditions and datasets – we used the image augmentation library, Albumentations [41] with the default configuration to apply several augmentations such as random fog, snow and rain. Table I shows the object detection accuracy in mAP for FRCNN and RetinaNet on multiple combination of *primary* and *secondary* dataset, respectively.

We adopted the CORAL [42] framework that uses a set of binary classifiers to train pm_{net} as an ordinal classifier. Each binary classifier predicts whether the per-window mAP is within a particular range. A decision threshold is used to control this prediction. The ordinal classifier has 5 classes from 0 to 4, each incrementally spanning 0.2 per-window mAP. In this case, class 1 is equivalent per-window mAP below 0.4. In all of the experiments, 0.4 is used as the critical threshold to train and evaluate the pm_{net} . Besides, 0.5 intersection over union has been used to calculate the mAP. We used the Adam optimizer [43] and an initial learning rate of 0.001 with batch size 32.

For all of the following experiments, we use a sliding window of 10 frames. We empirically found that this value

TABLE I: Object detection accuracy in mAP for FRCNN and RetinaNet network on multiple primary and secondary dataset for detecting vehicle and pedestrian.

Dataset		Object Detector	
Primary	Secondary	FRCNN	RetinaNet
kitti	kitti	66.00	60.58
kitti	bdd	44.81	42.60
kitti	waymo	44.03	43.57
bdd	kitti	42.70	43.88
bdd	bdd	52.45	65.49
bdd	waymo	47.15	49.20

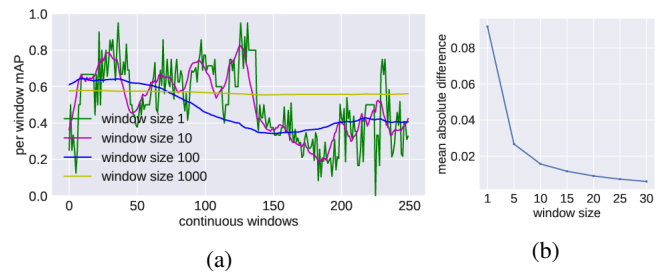


Fig. 4: (a) Per-window mAP for multiple lengths of continuous windows. (b) Mean absolute difference between two consecutive per-window mAP for different length of continuous windows.

provides a balance between the high sensitivity of smaller windows and the smoothing effect of large windows, as shown in Fig. 4.

D. Evaluation Metrics

We used mean absolute error (MAE), root mean squared error (RMSE), and zero-one error (ZOE) [44], which is the fraction of incorrect classification, as the evaluation metric for pm_{net} ordinal classification task. To compare with the baselines and to evaluate how well the pm_{net} can detect critical mAP label, we used true positive rate at 5% false positive rate (TPR@FPR5), false positive rate at 95% true positive rate (FPR@TPR95) and area under the ROC curve (AUROC) metric.

E. Baseline Approaches

Baseline 1: In [32], Ramanagopal et. al. proposed an approach to identify perception failure of an object detection system. They used manually selected features like bounding box confidence and their mean and median overlap to identify false negative instances generated by an object detector.

Following their approach, in this baseline, we extract a set of features from each image after performing the object detection. This set includes mean and median of all detected bounding box confidences, mean and median overlap, width and height of all detected bounding boxes on a normalized scale. We extracted these features from all images of each window and concatenated them together to generate a one-dimensional feature corresponding to the window. Next, each mAP per-window is converted into a binary label using a critical threshold of 0.4. Any mAP lower than this threshold is assigned to the positive class; otherwise, the negative. Next, we train a fully connected binary classifier to predict the probability of each window to be assigned in the positive or negative class.

Baseline 2: In this baseline, we are using internal features from the last convolutional layer of a trained object detector backbone instead of handcrafted features. After each inference, we collect the 3D features from the final backbone layer and apply the average pooling technique to convert that 3D features into 1D. After concatenating all 1D features from all the images of a window, we get a feature corresponding to that window. Using the critical threshold discussed in baseline 1, we assign each window into positive and negative classes. Then a fully connected binary classifier is trained to predict these classes from the window feature.

We use class 1, which is equivalent to the critical threshold of 0.4, to treat our ordinal classifier output as a binary classification. Consequently, classes from 0 to 1 and 2 to 4 are assigned to positive and negative classes, respectively. This conversion allows us to compare our ordinal classifier with the binary classifier based baselines.

V. EVALUATION AND RESULTS

In this section, we summarize how well the proposed performance monitoring network works as an ordinal classifier. Later, we evaluate the proposed network’s accuracy to detect when the per-window mAP drops below the critical threshold of 0.4.

Experiment 1: Table II shows the pm_{net} ordinal classification accuracy for our proposed approach, Baseline 1 and Baseline 2 using MAE, RMSE and ZOE metric for four different dataset settings. Here, od_{net} is trained using FRCNN

TABLE II: MAE, RMSE and ZOE score for baselines and pm_{net} trained using features collected from FRCNN.

Metric	Datasets			Ours	Base-line 2	Base-line 1
	Primary	Secondary	Test			
MAE↓	bdd	kitti	waymo	0.346	0.378	0.574
	bdd	waymo	kitti	0.181	0.375	0.409
	kitti	bdd	waymo	0.302	0.317	0.538
	kitti	waymo	bdd	0.241	0.316	0.446
RMSE↓	bdd	kitti	waymo	0.594	0.611	0.819
	bdd	waymo	kitti	0.428	0.618	0.656
	kitti	bdd	waymo	0.569	0.595	0.783
	kitti	waymo	bdd	0.496	0.603	0.739
ZOE↓	bdd	kitti	waymo	0.341	0.367	0.573
	bdd	waymo	kitti	0.182	0.356	0.386
	kitti	bdd	waymo	0.346	0.440	0.592
	kitti	waymo	bdd	0.269	0.369	0.513

and pm_{net} is trained and evaluated using FRCNN backbone features. The second dataset setting for all metrics shows pm_{net} error for ordinal classifying od_{net} performance on the KITTI *test* dataset. od_{net} and pm_{net} are trained using *primary* training dataset BDD and *secondary* training dataset Waymo, respectively. This setting demonstrates the lowest error in all the dataset settings.

Table III presents pm_{net} error metric for similar dataset settings as Table II. Here, od_{net} is trained using RetinaNet object detection network and pm_{net} is trained and evaluated using RetinaNet backbone features. In this table, *primary* training dataset BDD, *secondary* training dataset Waymo and *test* dataset KITTI demonstrates the lowest error than other dataset settings. This observation is consistent with Table II and suggests that the large diversity of BDD and Waymo dataset are effective for the performance monitoring of pm_{net} in the KITTI dataset.

Experiment 2: This experiment compares the proposed performance monitoring network with the baselines.

During the pm_{net} evaluation, the decision threshold is varied from 0 to 1 to produce the 5 class ordinal prediction for each threshold. Later, using the critical threshold, the ordinal class prediction is converted to a binary prediction to compute the TPR and FPR. Therefore, each decision threshold generates a pair of TPR, FPR and using these metrics; we calculate the TPR@FPR5, FPR@TPR95 and AUROC for our proposed approach.

As the two baselines use a binary classifier approach, we can use their predicted positive class probability and corresponding ground truth to calculate the TPR@FPR5, FPR@TPR95 and AUROC metric.

Table IV shows the comparison between pm_{net} and the two baselines using multiple metrics. For this table, the od_{net} is trained using FRCNN and the pm_{net} is trained and evaluated using FRCNN backbone features. In terms of TPR@FPR5, pm_{net} outperforms both of the baselines. While the maximum TPR@FPR5 for pm_{net} over four dataset settings is 0.922, baseline 1 and 2 reach at maximum 0.214 and 0.513 respectively. For FPR@TPR95, the minimum score for our proposed approach is 0.054. However, the minimum FPR@TPR95 for baseline 1 and 2 is 0.707 and 0.457, respectively. In AUROC metrics, pm_{net} performs

TABLE III: MAE, RMSE and ZOE score for baselines and pm_{net} trained using features collected from RetinaNet.

Metric	Datasets			Ours	Base-line 2	Base-line 1
	Primary	Secondary	Test			
MAE↓	bdd	kitti	waymo	0.307	0.418	0.532
	bdd	waymo	kitti	0.272	0.387	0.487
	kitti	bdd	waymo	0.275	0.326	0.501
	kitti	waymo	bdd	0.290	0.433	0.501
RMSE↓	bdd	kitti	waymo	0.601	0.675	0.833
	bdd	waymo	kitti	0.523	0.548	0.744
	kitti	bdd	waymo	0.554	0.639	0.771
	kitti	waymo	bdd	0.561	0.719	0.784
ZOE↓	bdd	kitti	waymo	0.281	0.480	0.524
	bdd	waymo	kitti	0.259	0.390	0.498
	kitti	bdd	waymo	0.266	0.307	0.472
	kitti	waymo	bdd	0.277	0.429	0.486

better than the baselines by obtaining 0.929 while the maximum AUROC of both baselines is 0.610. Although we have referred only to the maximum score of each individual metrics from the four dataset settings, our proposed approach outperforms the baselines in all metrics and dataset settings.

Table V represents the comparative accuracy among pm_{net} and two other baselines. Here, the underlying object detector is trained using the RetinaNet network and the corresponding performance monitoring network is trained and evaluated using features collected from the RetinaNet backbone. In this case, for the TPR@FPR5 metric, the maximum score that our proposed approach achieves out of four dataset settings is 0.953 while the maximum of two baselines among these four settings is 0.708. In the case of FPT@TPR95 and AUROC, our proposed approach outperforms both of the baselines. Fig. 5 demonstrates the multiple example of performance drop when the object detector is trained and tested on *primary* and *secondary* dataset, respectively. In all cases, the mAP is lower than the critical threshold, and our performance monitoring network flags them correctly.

This experimental result demonstrates the effectiveness of internal features of an object detector for performance monitoring task. Although Baseline 1 and Baseline 2 can be used for performance monitoring, our proposed approach outperforms them because of the cascaded architecture’s internal feature usage. Here, the cascaded architecture can capture the gradual change in the per-window mAP better than the baselines. Moreover, instead of using features only from the last layer of the object detection backbone, our proposed approach extracts internal features from all convolutional layers. This approach derives global and local multi-level semantic features for better performance monitoring.

Experiment 3: In order to monitor object detection performance online, we are required to simultaneously use the performance monitoring network along with the object detection system. Hence, the inference time and GPU memory requirement of pm_{net} should be minimal for practical usage. On average pm_{net} and od_{net} inference time is 3.34 ± 0.126 ms and 28.11 ± 0.404 ms in our TITAN V GPU workstation.

TABLE IV: pm_{net} comparison with other baselines. Here, pm_{net} is trained using FRCNN backbone features.

Metric	Datasets			Ours	Base-line 2	Base-line 1
	Primary	Secondary	Test			
TPR@	bdd	kitti	waymo	0.882	0.270	0.214
FPR5 \uparrow	bdd	waymo	kitti	0.922	0.378	0.080
	kitti	bdd	waymo	0.916	0.320	0.157
	kitti	waymo	bdd	0.897	0.513	0.133
FPR@	bdd	kitti	waymo	0.064	0.775	0.707
TPR95 \downarrow	bdd	waymo	kitti	0.093	0.557	0.777
	kitti	bdd	waymo	0.133	0.766	0.827
	kitti	waymo	bdd	0.054	0.457	0.948
AUROC	bdd	kitti	waymo	0.873	0.644	0.648
\uparrow	bdd	waymo	kitti	0.891	0.589	0.537
	kitti	bdd	waymo	0.892	0.610	0.573
	kitti	waymo	bdd	0.929	0.560	0.528



Fig. 5: Example of performance drop encountered by the object detection system. Red and Blue coloured boxes represent the false negative and false positive error made by the object detector in each input frame. 1st and 2nd rows represent Faster RCNN and RetinaNet detection performance for primary dataset KITTI and secondary dataset BDD. 3rd and 4th rows show Faster RCNN and RetinaNet performance for primary dataset BDD and secondary dataset Waymo. In all cases, the mAP is lower than 0.4, and detection confidence is higher than 0.5.

Besides, pm_{net} uses 243 MB of GPU memory which is 20.81% of memory used by the od_{net} .

VI. CONCLUSION

As deep learning-based object detection becomes essential components of a wide variety of robotic systems, the ability to continuously assess and monitor their performance during the deployment phase becomes critical to ensure the safety and reliability of the whole system. In this paper, we proposed a specialized performance monitoring network that can predict the quality of the mAP of the object detector, which

TABLE V: pm_{net} comparison with other baselines. Here, pm_{net} is trained using RetinaNet backbone features.

Metric	Datasets			Ours	Base-line 2	Base-line 1
	Primary	Secondary	Test			
TPR@	bdd	kitti	waymo	0.875	0.228	0.157
FPR5 \uparrow	bdd	waymo	kitti	0.953	0.380	0.080
	kitti	bdd	waymo	0.915	0.576	0.214
	kitti	waymo	bdd	0.889	0.708	0.133
FPR@	bdd	kitti	waymo	0.098	0.576	0.827
TPR95 \downarrow	bdd	waymo	kitti	0.109	0.765	0.777
	kitti	bdd	waymo	0.053	0.479	0.707
	kitti	waymo	bdd	0.076	0.911	0.948
AUROC	bdd	kitti	waymo	0.860	0.567	0.573
\uparrow	bdd	waymo	kitti	0.917	0.596	0.537
	kitti	bdd	waymo	0.915	0.564	0.648
	kitti	waymo	bdd	0.873	0.746	0.528

can be used to inform downstream components in the robotic system about the expected object detection reliability. We show the effectiveness of our approach using a combination of different autonomous driving datasets and object detectors.

REFERENCES

- [1] Z. Tian, C. Shen, H. Chen, and T. He, “FCOS: Fully Convolutional One-stage Object Detection,” in *Proceedings of the IEEE international conference on computer vision*, 2019, pp. 9627–9636.
- [2] S. Ren, K. He, R. Girshick, and J. Sun, “Faster R-CNN: Towards Real-time Object Detection With Region Proposal Networks,” in *Advances in neural information processing systems*, 2015, pp. 91–99.
- [3] W. Liu, D. Anguelov, D. Erhan, C. Szegedy, S. Reed, C.-Y. Fu, and A. C. Berg, “SSD: Single Shot Multibox Detector,” in *European conference on computer vision*. Springer, 2016, pp. 21–37.
- [4] K. Duan, S. Bai, L. Xie, H. Qi, Q. Huang, and Q. Tian, “CenterNet: Keypoint Triplets for Object Detection,” *2019 IEEE/CVF International Conference on Computer Vision (ICCV)*, pp. 6568–6577, 2019.
- [5] A. Bochkovskiy, C.-Y. Wang, and H.-Y. M. Liao, “YOLOv4: Optimal Speed and Accuracy of Object Detection,” *ArXiv*, vol. abs/2004.10934, 2020.
- [6] K. He, R. B. Girshick, and P. Dollár, “Rethinking ImageNet Pre-Training,” *2019 IEEE/CVF International Conference on Computer Vision (ICCV)*, pp. 4917–4926, 2019.
- [7] Z. Cai and N. Vasconcelos, “Cascade R-CNN: Delving Into High Quality Object Detection,” *2018 IEEE/CVF Conference on Computer Vision and Pattern Recognition*, pp. 6154–6162, 2018.
- [8] Z. Li, C. Peng, G. Yu, X. Zhang, Y. Deng, and J. Sun, “DetNet: A Backbone network for Object Detection,” *ArXiv*, vol. abs/1804.06215, 2018.
- [9] T.-Y. Lin, P. Goyal, R. B. Girshick, K. He, and P. Dollár, “Focal Loss for Dense Object Detection,” *2017 IEEE International Conference on Computer Vision (ICCV)*, pp. 2999–3007, 2017.
- [10] N. Carion, F. Massa, G. Synnaeve, N. Usunier, A. M. Kirillov, and S. Zagoruyko, “End-to-End Object Detection with Transformers,” *ArXiv*, vol. abs/2005.12872, 2020.
- [11] A. C. Morris, “Robotic Introspection for Exploration and Mapping of Subterranean Environments,” Ph.D. dissertation, Carnegie Mellon University, The Robotics Institute, 2007.
- [12] H. Grimmer, R. Triebel, R. Paul, and I. Posner, “Introspective Classification for Robot Perception,” *The International Journal of Robotics Research*, vol. 35, no. 7, pp. 743–762, 2016.
- [13] R. Triebel, H. Grimmer, R. Paul, and I. Posner, “Driven Learning for Driving: How Introspection Improves Semantic Mapping,” in *ISRR*, 2013.
- [14] P. Zhang, J. Wang, A. Farhadi, M. Hebert, and D. Parikh, “Predicting Failures of Vision Systems,” in *Proceedings of the IEEE Conference on Computer Vision and Pattern Recognition*, 2014, pp. 3566–3573.
- [15] S. Daftry, S. Zeng, J. A. Bagnell, and M. Hebert, “Introspective Perception: Learning to Predict Failures in Vision Systems,” in *2016 IEEE/RSJ International Conference on Intelligent Robots and Systems (IROS)*. IEEE, 2016, pp. 1743–1750.
- [16] P. Wang and N. Vasconcelos, “Towards Realistic Predictors,” in *Proceedings of the European Conference on Computer Vision (ECCV)*, 2018, pp. 36–51.
- [17] C. Gurau, D. Rao, C. H. Tong, and I. Posner, “Learn From Experience: Probabilistic Prediction of Perception Performance to Avoid Failure,” *The International Journal of Robotics Research*, vol. 37, pp. 981 – 995, 2018.
- [18] H. Jiang, B. Kim, and M. R. Gupta, “To Trust or Not to Trust A Classifier,” in *NeurIPS*, 2018.
- [19] D. Hendrycks and K. Gimpel, “A Baseline for Detecting Misclassified and Out-of-Distribution Examples in Neural Networks,” *ArXiv*, vol. abs/1610.02136, 2017.
- [20] C. Corbière, N. Thome, A. Bar-Hen, M. Cord, and P. Pérez, “Addressing Failure Prediction by Learning Model Confidence,” in *Advances in Neural Information Processing Systems*, 2019, pp. 2902–2913.
- [21] Y. Gal and Z. Ghahramani, “Dropout as a Bayesian Approximation: Representing Model Uncertainty in Deep Learning,” in *ICML*, 2016.
- [22] P.-Y. Huang, W. T. Hsu, C.-Y. Chiu, T.-F. Wu, and M. Sun, “Efficient Uncertainty Estimation for Semantic Segmentation in Videos,” in *ECCV*, 2018.
- [23] T. Devries and G. W. Taylor, “Leveraging Uncertainty Estimates for Predicting Segmentation Quality,” *ArXiv*, vol. 1807.00502, 2018.
- [24] D. Hendrycks and K. Gimpel, “A baseline for detecting misclassified and out-of-distribution examples in neural networks,” *arXiv preprint arXiv:1610.02136*, 2016.
- [25] S. Liang, Y. Li, and R. Srikant, “Enhancing the Reliability of Out-of-Distribution Image Detection in Neural Networks,” *arXiv preprint arXiv:1706.02690*, 2017.
- [26] D. Hendrycks, M. Mazeika, and T. Dietterich, “Deep anomaly detection with outlier exposure,” *arXiv preprint arXiv:1812.04606*, 2018.
- [27] K. Lee, H. Lee, K. Lee, and J. Shin, “Training confidence-calibrated classifiers for detecting out-of-distribution samples,” *arXiv preprint arXiv:1711.09325*, 2017.
- [28] K. Lee, K. Lee, H. Lee, and J. Shin, “A simple unified framework for detecting out-of-distribution samples and adversarial attacks,” *arXiv preprint arXiv:1807.03888*, 2018.
- [29] D. Miller, L. Nicholson, F. Dayoub, and N. Sünderhauf, “Dropout Sampling for Robust Object Detection in Open-Set Conditions,” *2018 IEEE International Conference on Robotics and Automation (ICRA)*, pp. 1–7, 2018.
- [30] B. Cheng, Y. Wei, H. Shi, R. S. Feris, J. Xiong, and T. S. Huang, “Decoupled Classification Refinement: Hard False Positive Suppression for Object Detection,” *ArXiv*, vol. abs/1810.04002, 2018.
- [31] Q. M. Rahman, N. Sünderhauf, and F. Dayoub, “Did You Miss the Sign? A False Negative Alarm System for Traffic Sign Detectors,” *2019 IEEE/RSJ International Conference on Intelligent Robots and Systems (IROS)*, pp. 3748–3753, 2019.
- [32] M. S. Ramanagopal, C. Anderson, R. Vasudevan, and M. Johnson-Roberson, “Failing to Learn: Autonomously Identifying Perception Failures for Self-Driving Cars,” *IEEE Robotics and Automation Letters*, vol. 3, pp. 3860–3867, 2018.
- [33] A. Azulay and Y. Weiss, “Why Do Deep Convolutional Networks Generalize So Poorly to Small Image Transformations?” *arXiv preprint arXiv:1805.12177*, 2018.
- [34] J. S. Cardoso and J. F. Costa, “Learning to Classify Ordinal Data: The Data Replication Method,” *Journal of Machine Learning Research*, vol. 8, no. Jul, pp. 1393–1429, 2007.
- [35] A. Geiger, P. Lenz, and R. Urtasun, “Are We Ready for Autonomous Driving? The KITTI Vision Benchmark Suite,” in *Conference on Computer Vision and Pattern Recognition (CVPR)*, 2012.
- [36] F. Yu, W. Xian, Y. Chen, F. Liu, M. Liao, V. Madhavan, and T. Darrell, “BDD100k: A Diverse Driving Video Database With Scalable Annotation Tooling,” *arXiv preprint arXiv:1805.04687*, vol. 2, no. 5, p. 6, 2018.
- [37] P. Sun, H. Kretschmar, X. Dotiwalla, A. Chouard, V. Patnaik, P. Tsui, J. Guo, Y. Zhou, Y. Chai, B. Caine, V. Vasudevan, W. Han, J. Ngiam, H. Zhao, A. Timofeev, S. Ettinger, M. Krivokon, A. Gao, A. Joshi, Y. Zhang, J. Shlens, Z. Chen, and D. Anguelov, “Scalability in Perception for Autonomous Driving: Waymo Open Dataset,” in *Proceedings of the IEEE/CVF Conference on Computer Vision and Pattern Recognition (CVPR)*, June 2020.
- [38] T.-Y. Lin, P. Goyal, R. Girshick, K. He, and P. Dollár, “Focal Loss for Dense Object Detection,” in *Proceedings of the IEEE international conference on computer vision*, 2017, pp. 2980–2988.
- [39] T.-Y. Lin, M. Maire, S. Belongie, J. Hays, P. Perona, D. Ramanan, P. Dollár, and C. L. Zitnick, “Microsoft COCO: Common Objects in Context,” in *European conference on computer vision*. Springer, 2014, pp. 740–755.
- [40] K. He, X. Zhang, S. Ren, and J. Sun, “Deep Residual Learning for Image Recognition,” in *Proceedings of the IEEE conference on computer vision and pattern recognition*, 2016, pp. 770–778.
- [41] A. Buslaev, V. I. Iglovikov, E. Khvedchenya, A. Parinov, M. Druzhinin, and A. A. Kalinin, “Albumentations: Fast and flexible image augmentations,” *Information*, vol. 11, no. 2, 2020. [Online]. Available: <https://www.mdpi.com/2078-2489/11/2/125>
- [42] W. Cao, V. Mirjalili, and S. Raschka, “Rank-consistent Ordinal Regression for Neural Networks,” *arXiv preprint arXiv:1901.07884*, 2019.
- [43] D. P. Kingma and J. Ba, “Adam: A Method for Stochastic Optimization,” *arXiv preprint arXiv:1412.6980*, 2014.
- [44] K. Dembczyński, W. Kotłowski, and R. Stowiński, “Ordinal Classification with Decision Rules,” in *International Workshop on Mining Complex Data*. Springer, 2007, pp. 169–181.